Available online www.jsaer.com

***Journal of Scientific and Engineering Research*, 2022, 9(3):110-120**

Research Article

ISSN: 2394-2630
CODEN(USA): JSERBR

MHD Active Control Flow of Nanoparticles with Buoyancy and Variable Viscosity and Thermal Conductivity

Kelvin O. Ogboru[1], Azeez. A. Waheed[2], Akindele. M. Okedoye[1]

[1]Department of Mathematics, Federal University of Petroleum Resources, Effurun, Nigeria
[2]Department of Mathematics, Lead City University, Ibadan, Oyo State Nigeria
Corresponding Author: okedoye.akindele @fupre.edu.ng

Abstract The motivation for this research paper is to analyze MHD active flow of nanoparticles with buoyancy and variable viscosity and thermal conductivity. Buongiorno's model is used to investigate the flow, heat, and mass transfer of a nanofluid over an abruptly moving flat plate. The effects of Brownian motion and thermophoresis on the volume fraction of nanoparticles are actively controlled on the boundary rather than passively managed in prior investigations. The flow's partial differential equations are reduced to a system of nonlinear ordinary differential equations, which are then solved using MAPLE 2021's shooting technique, and the resulting system is solved using the Runge-kutta Fehlberg method. With graphical representation, the effect of various important physical parameters on velocity, energy, concentration, skin friction coefficient, Nusselt number, and Sherwood number is investigated. A table is also given that provides the results of different parameters on local Nusselt and Sherwood numbers. The active control model can be used to control the boundary layer thickness as well as the rate of mass transfer at the wall.

Keywords Buoyancy effect, MHD, Nanofluid, Porous Medium, Dufour, Ohmic heating, thermal radiation. Thermo-physical properties, Richardson extrapolation
MSC 2020: 76A05, 76D05, 76W05

1. Introduction

Flow control is a key topic of fluid dynamics that is rapidly evolving. It refers to a minor alteration in a configuration that has a significant technical benefit, such as reducing drag, increasing lift, improving mixing, or reducing noise. Passive or active devices may be used to effect this transformation. Turbulators and roughness elements are examples of passive devices that are stable and require no energy to operate. Active control, according to Yousefi and Saleh (2015), necessitates actuators that can be controlled in a time-dependent manner and demand energy. Valves and plasma actuators are two examples. The actuation instruction might be pre-programmed (open-loop control) or based on sensors that monitor the flow status (closed-loop control).

The performance of airplane wings has a significant impact on runway length, approach speed, climb rate, cargo capacity, and operation range, as well as community noise and emission levels. Flow separation, which is highly dependent on the aerodynamic design of the airfoil profile, degrades wing performance frequently. Active control systems are considered to be a more advanced technology; their concept is based on real-time processing that allows them to respond to excitation using sensors built into the device. These sensors gather data on excitation and structural response, then adapt the device's behavior based on the information gathered (Saaed & Nikolakopoulos, 2015, Soong & Spencer, 2002). Stable suction or blowing are examples of active flow control methods.

Xiao Quab and Yanfeng Zhangab investigated the control mechanism of a fluidic oscillator in the suppression of non-reattachment separation of a boundary layer from an ultra-high-lift, aft-loaded, low-pressure turbine using large eddy simulation (LES) at low Reynolds numbers (2021). The fluidic oscillator's internal flow properties were investigated, with a focus on the influence mechanism of the pulse jet from the fluidic oscillator on boundary layer separation and transition. According to the author, the fluidic oscillator's pulse jet formed a stream-wise vortex pair above the blade suction surface, which promoted an interchange of momentum between the blade suction surface's boundary layer and the main flow and effectively reduced boundary layer separation.

M. Habibnia and J. Pascoa (2021) demonstrated that actively managing pitching oscillations and rotational speeds increased the performance of cycloidal rotors. Yousefi and Saleh used computational fluid dynamics (CFD) and artificial neural networks (ANN) in their optimization analysis for hover-state operations rather than take-off mode subsurface effects (2015). The optimum operational state for a 30 and 500 (rpm) pitch angle and rotating speed, respectively, is predicted using CFD simulations.

This active control concept proved to be a viable method for increasing cyclorotor efficiency by an average of 12%.

In many practical situations nowadays, there are situations in which we have to work out with different types of nanoparticles. These nano sized particles play a crucial role in controlling the different thermos physical properties of different fluids involved. Most of the fluids in practice such as water, ethylene, glycol, kerosene oil, engine oil are the poor conductors of heat. Lower thermal conductivity and other thermal characteristics are a major contributing factor. Nanoparticles are added to the base fluids to solve this problem and improve the thermal properties of these fluids. To get a concrete analysis of these nanoparticle-based nanofluids, many researchers studied and proposed various models.

S.T. Mohyud-Din, U. Khan, N. Ahmed, and Bandar Bin-Mohsin (2017) investigated the diffusion of vorticity over a suddenly moving flat surface, while K.R. Rajagopal and T.Y. Na (1983) extended the standard problem to non-Newtonian fluids. Over the years, many researchers studied several properties of velocity field in Stokes' problem. Many studies can be seen in literature on Stokes' problem H. Schlichting, (1968), Rajagopal e.tal (1983), M. Turkyilmazoglu (2015), M. Turkyilmazoglu, (2012), Seth e.tal. (2011), Seth e.tal. (2012), Seth e.tal. (2013), Nandkeolyar e.tal (2013), Seth e.tal. (2014), Seth e.tal. (2015), Seth e.tal. (2015), Seth e.tal. (2016), Seth e.tal. (2015), V.M. Soundalgekar (1981), P. Puri (1984) and P. Puri, M. Jordan (1999). Naseem Uddin et al. (2012) recently published a study of nanofluids caused by a quickly moving plate, after pioneering work in nanofluids. The Buongiorno model was used by Rosali et al. (2014) to investigate the impact of Brownian motion and thermophoresis on heat and mass transfer in nanofluids.

Nield and Kuznetsov (2014, 2014, and 2014) proposed a new revised model for the concentration profile at the wall that included the zero flux boundary condition. The effects of Brownian motion and thermophoresis are included in this boundary condition, allowing the nanofluid particle fraction to be passively regulated at the wall. They also stated that this model is physically more realistic than previous ones.The model presented by Nield and Kuznetsov (2014, 2014, and 2014) is utilized by Syed et al. (2018) to explore the flow behavior of a nanofluid across a quickly moving flat plate. Brownian motion and thermophoresis effects are accounted for in the zero flux boundary condition. The effects of buoyancy, Lorentz force, heat source, and chemical reaction were not taken into account. By extending the work of Syed et al. (2018) to include buoyancy, Lorentz force, heat source, chemical reaction, as well as Variable Viscosity and Thermal Conductivity, we hope to investigate Heat and Mass Transfer Effects on MagnetoHydroDynamic Flow of Nanoparticles with Buoyancy and Variable Viscosity and Thermal Conductivity.

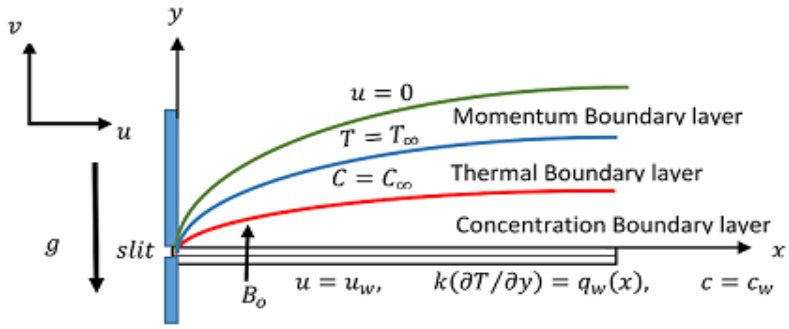

Figure 1: Schematic diagram for the flow problem

$$q_w(x) = h_f(T_f - T)$$

2. Governing Equations

Consider the flow of a Newtonian nanofluid lying over an impulsively started heated plate. Cartesian coordinate system is taken to describe the flow behavior. x and y respectively are the coordinates along and normal to the plate. Initially (at time $t = 0$), the plate is starts moving with a constant velocity U_∞. The temperature of the plate is kept constant at T w, while the nanoparticle volume fraction is kept constant at C w. The temperature and the nanoparticle volume fraction are represented by T_∞ and C_∞, respectively, at a great distance from the plate. In the y-direction, a uniform time-dependent transverse magnetic field is applied. The magnetic field strength is assumed to be $B = B_0$. The induced magnetic field is thought to be insignificant in comparison to the applied magnetic field and is therefore ignored.

The flow problem is depicted schematically in Figure 1.

For the problem considered here we define the velocity and the stress fields of the following form

$$V = [u(y,t), 0, 0]$$

The physical variables are functions of y and t only. Therefore, the only velocity component is in y -direction. The continuity equation could be expressed as follows based on the above assumption:

$$\frac{\partial v}{\partial y} = 0 \tag{1}$$

Under the Boussinesq's approximation, the fluid momentum, energy and species equations in the neighbourhood of the plate is described by the following respectively

$$\rho_f\left(\frac{\partial u}{\partial t} + v\frac{\partial u}{\partial y}\right) = -\frac{\partial p}{\partial x} + \frac{\partial u}{\partial y}\left(\mu_T\frac{\partial u}{\partial y}\right) + g\beta_T(T - T_\infty) + g\beta_C(C - C_\infty) - \sigma B_0^2 u, \tag{2}$$

$$\rho C_p\left(\frac{\partial T}{\partial t} + v\frac{\partial T}{\partial y}\right) = \frac{\partial T}{\partial y}\left(K_T\frac{\partial T}{\partial y}\right) + \tau\left[D_B\left(\frac{\partial C}{\partial y}\frac{\partial T}{\partial y}\right) + \left(\frac{D_T}{T_\infty}\right)\left(\frac{\partial T}{\partial y}\right)^2\right] + Q(T - T_\infty), \tag{3}$$

$$\frac{\partial C}{\partial t} + v\frac{\partial C}{\partial y} = D_B\left(\frac{\partial^2 C}{\partial y^2}\right) + \frac{D_T}{T_\infty}\left(\frac{\partial^2 T}{\partial y^2}\right) + A(C - C_\infty). \tag{4}$$

where, u is the velocity component along the $y-$axis, U_∞ is the velocity of the free stream, ρ_f is the density of base fluid, $v = \mu_f/\rho_f$ is kinematic viscosity, σ is electrical conductivity, B_0 magnetic field flux density, α thermal diffusivity, D_B is Brownian motion diffusion coefficient, D_T thermophoresis diffusion coefficient, T and C are fluid temperature and nanoparticle volume fraction, respectively, τ is the parameter defined by

$$\frac{(\rho c)_f}{(\rho c)_p},$$

where $(\rho c)_f$ is the heat capacity of the nanofluid and $(\rho c)_p$ is the effective heat capacity of the nanoparticle material.

Internal friction between the surface and the fluid particle causes variations in viscosity and thermal conductivity, thus it's reasonable to suppose that the mathematical formulation of thermal conductivity and viscosity as a function of temperature was examined.

We adopt the following assumptions for viscosity and thermal conductivity, which are comparable to those used by Wahab (2020):

$$\mu_T = \mu_f\big(a + b_1(T_\infty - T)\big), \qquad k_T = k_f\big(a_1 + b_2(T - T_\infty)\big), \tag{5}$$

For active control model, the initial and boundary conditions are obtained when $D_T = 0$, thus $C = C_w$. That is

$$\begin{aligned} t < 0: &\quad u = 0, v = v_w, T = T_w, C = C_w, \quad \text{for all } y \\ t \geq 0: &\quad u = U_0, T = T_w, C = C_w, \text{at } y = 0 \\ &\quad u \to 0, T \to T_\infty, C \to C_\infty, \text{as } y \to \infty \end{aligned} \tag{6}$$

This condition's main goal is to actively regulate the nanoparticle volume fraction near the boundary.

2.1 Non-Dimensionlisation

The following non-dimensional variables are used in the mathematical analysis of the problem for the active control model.

$$\left.\begin{aligned} y' = \frac{y}{\delta}, u' = \frac{u}{U_0}, v' = \frac{v}{U}\frac{L}{\delta}, p' = \frac{p}{\rho U^2}, t' = t\frac{U_0}{L}, U' = \frac{U}{U_0}, \omega' = \frac{4\omega L}{U_0}, \\ V = \frac{U_1}{U_0}, (T - T_\infty) = \frac{R_G T_\infty^2}{E_a}\theta(t,y), (C - C_\infty) = (C_w - C_\infty)\phi(t,y) \end{aligned}\right\} \tag{7}$$

At free stream

$$u \to U(t) = 1 + nt, T \to T_\infty, C \to C_\infty$$

Where is a parameter defined by

$$n = \frac{4\rho_f U_0 G}{L\sigma B_0^2 + 4\rho_f U_0}$$

$$\rho_f\left(\frac{\partial U}{\partial t}\right) = -\frac{\partial p}{\partial x} - \sigma B_0^2 U, \tag{8}$$

Equation (8) implies

$$-\frac{\partial p}{\partial x} = \rho_f\left(\frac{\partial U}{\partial t}\right) + \sigma B_0^2 U \tag{9}$$

Hence by equation (9), equation (2) becomes

$$\begin{aligned} \rho_f\left(\frac{\partial u}{\partial t} + v\frac{\partial u}{\partial y}\right) = \rho_f\left(\frac{\partial U}{\partial t}\right) + \frac{\partial u}{\partial y}\left(\mu_T\frac{\partial u}{\partial y}\right) + g\beta_T(T - T_\infty), \\ + g\beta_C(C - C_\infty) - \sigma B_0^2(u - U) \end{aligned} \tag{10}$$

Using equation (7) in equations (1), (3), (4) and (10) respectively, we have

$$\begin{aligned} \frac{\partial\theta(t,y)}{\partial t'} + v'\frac{\partial\theta(t,y)}{\partial y'} = \frac{1}{Pr}\frac{\partial}{\partial y'}\left(\big(\alpha + \varphi\theta(t,y)\big)\frac{\partial\theta(t,y)}{\partial y'}\right) \\ + \frac{\pi}{\sigma(t)^2}\left[Nb\left(\frac{\partial\phi(t,y)}{\partial y'}\frac{\partial\theta(t,y)}{\partial y'}\right) + Nt\left(\frac{\partial\theta(t,y)}{\partial y'}\right)^2\right] + \frac{\beta}{Pr}\theta(t,y) \end{aligned} \tag{12}$$

$$\frac{\partial\phi(y)}{\partial t'} + v'\frac{\partial\phi(y)}{\partial y'} = \frac{1}{Sc\sigma(t)^2}\frac{\partial^2\phi(y)}{\partial y'^2} + \frac{1}{Sc\sigma(t)^2}\frac{Nt}{Nb}\frac{\partial^2\theta(y)}{\partial y'^2} + \Lambda\phi(y) \tag{13}$$

$$\begin{aligned} \frac{\partial u'}{\partial t'} + v'\frac{\partial u'}{\partial y'} = \frac{dU'}{dt} + \frac{\nu}{\sigma(t)^2}\frac{\partial}{\partial y'}\left(\big(\zeta - \gamma\theta(t,y)\big)\frac{\partial u'}{\partial y'}\right) \\ + Grt(\theta(t,y) + N\phi(t,y)) - M(u' - U') \end{aligned} \tag{14}$$

The initial and boundary conditions for passive control model becomes

$$\begin{aligned} t < 0: &\quad u' = 0, v' = s, \qquad \theta(t,y) = 1, \phi(t,y) = 1 \qquad \text{for all } y \\ t \geq 0: &\begin{cases} u' = 1, v' = s, \theta(t,y) = 1, Nb\dfrac{\partial\phi(t,y)}{\partial y'} + Nt\dfrac{\partial\theta(t,y)}{\partial y'} = 0, \text{at } y' = 0 \\ u' \to 0, \theta(t,y) \to 0, \phi(t,y) \to 0, \qquad \text{as } y' \to \infty \end{cases} \end{aligned} \tag{16}$$

Dropping primes, system of equations (12) – (15) in non-dimensional form of the governing equations in terms of dimensionless variables are:

$$\frac{\partial v}{\partial y} = 0 \tag{17}$$

$$\frac{\partial u}{\partial t} + v\frac{\partial u}{\partial y} = \frac{dU}{dt} + \frac{\nu}{\sigma(t)^2}\frac{\partial}{\partial y}\left(\left(\zeta - \gamma\theta(t,y)\right)\frac{\partial u}{\partial y}\right) + Grt(\theta(t,y) + N\phi(t,y)) - M(u-U) \tag{18}$$

$$\frac{\partial \theta(t,y)}{\partial t} + v\frac{\partial \theta(t,y)}{\partial y} = \frac{1}{Pr}\frac{1}{\sigma(t)^2}\frac{\partial}{\partial y}\left(\left(\alpha + \varphi\theta(t,y)\right)\frac{\partial \theta(t,y)}{\partial y}\right) + \frac{\pi}{\sigma(t)^2}\left[Nb\left(\frac{\partial \phi(t,y)}{\partial y}\frac{\partial \theta(t,y)}{\partial y}\right) + Nt\left(\frac{\partial \theta(t,y)}{\partial y}\right)^2\right] + \frac{\beta}{Pr}\theta(t,y) \tag{19}$$

$$\frac{\partial \phi(y)}{\partial t} + v\frac{\partial \phi(y)}{\partial y} = \frac{1}{Sc\sigma(t)^2}\frac{\partial^2 \phi(y)}{\partial y^2} + \frac{1}{Sc\sigma(t)^2}\frac{Nt}{Nb}\frac{\partial^2 \theta(y)}{\partial y^2} + \Lambda\phi(y) \tag{20}$$

And the corresponding boundary conditions (16) becomes

$$\begin{aligned} t < 0:&\quad u = 0, v = s, \theta(t,y) = 1, \phi(t,y) = 1, \text{ for all } y \\ t \geq 0:&\quad \begin{cases} u = 1, v = s, \theta(t,y) = 1, \phi(t,y) = 1, \text{at } y = 0 \\ u \to 0, \theta(t,y) \to 0, \phi(t,y) \to 0, \quad \text{as } y \to \infty \end{cases} \end{aligned} \tag{21}$$

Where the dimensionless variable are

$$\left.\begin{aligned} \left(a + b_1(T_w - T_\infty)\right)\frac{L}{U_0} = \zeta, \frac{L}{U_0\rho c_p} = \pi, g\beta_T\frac{R_G T_\infty^2 L}{E_a \rho_f U_0^2} = Grt, \frac{L\sigma B_0^2}{\rho_f U_0} = M, \\ \frac{\beta_C(C_w - C_\infty)}{\epsilon T_\infty \beta_T} = N, \frac{k_0}{\rho c_p} = \frac{1}{Pr}, \frac{QL}{k_0 U_0} = \beta, b_1\frac{R_G T_\infty^2 L}{E_a U_0} = \gamma, b_2\frac{R_G T_\infty^2}{E_a U_0} = \varphi, \\ \frac{D_B}{\rho}\frac{L}{U_0} = \frac{1}{Sc}, \frac{AL}{\rho U_0} = \Lambda, , a_1\frac{L}{U_0} = \alpha, s = \frac{v_w L}{U\delta}, \frac{\tau D_B(C_w - C_\infty)}{\upsilon} = Nb, \frac{\tau D_T R_G T_\infty}{E_a \upsilon} = Nt \end{aligned}\right\} \tag{22}$$

Nt and Nb Brownian motion parameter and thermophoresis parameter, respectively.

2.2. **Rate of Heat and Mass Transfer at the wall**

The quantities of engineering interest are the local Nusselt number Nu and Sherwood number Sh. These parameters characterize the wall heat and nano mass transfer rates,

The quantities Skin friction, Nusselt and Sherwood Number are denoted by c_f, Nu and Sh respectively and are define as follows:

$$c_f = \frac{\tau_w}{\rho U_0^2}, \tag{23}$$

$$Nu = \frac{xq_w}{k_0(T_w - T_\infty)}, \tag{24}$$

$$Sh = \frac{xq_m}{D_B(C_w - C_\infty)} \tag{25}$$

where τ_w represents the skin friction along the surface, q_w the heat flux and q_m the concentration flux from the surface and are respectively given as

$$\left.\begin{aligned} \tau_w &= \mu(T)\left[\left(1 + \frac{1}{\beta c}\right)\frac{\partial u}{\partial y} + \frac{1}{\beta c^6}\left(\frac{\partial u}{\partial y}\right)^3\right]_{y=0}, \\ q_w &= \left[-k_T\frac{\partial u}{\partial y}\right]_{y=0}, \\ q_m &= \left[-D_B\frac{\partial C}{\partial y}\right]_{y=0} \end{aligned}\right\} \tag{26}$$

where U_0 q_m and q_w, represents the wall shear stress, mass flux and heat transfer respectively.

Using Equation (5) and (26) in (23) – (25) we have

$$c_f = \frac{\mu(T)}{\rho_f U_0^2}\left[\left(1 + \frac{1}{\beta c}\right)\frac{\partial u}{\partial y} + \frac{1}{\beta c^6}\left(\frac{\partial u}{\partial y}\right)^3\right]_{y=0}, \tag{27}$$

$$Nu = \frac{xE_a}{k_0 R_G T_\infty^2}\left[-k_T\frac{\partial T}{\partial y}\right]_{y=0}, \tag{28}$$

$$Sh = \frac{x}{D_B(C_w - C_\infty)}\left[-D_B\frac{\partial C}{\partial y}\right]_{y=0} \tag{29}$$

Using equation (8), equations (27)-(29) are transform in dimensionless form as follows

$$c_f = \frac{1}{\delta^2}\left(\zeta - \gamma\theta(t,y)\right)\left[H\frac{\partial u'}{\partial y'} + \Omega\left(\frac{\partial u'}{\partial y'}\right)^3\right]_{y=0}, \tag{30}$$

Also

$$Nu = -\frac{1}{\delta^2}\left[\left(\alpha + \varphi\theta(t,y)\right)\frac{\partial\,\theta(t,y)}{\partial y'}\right]_{y=0} \tag{31}$$

$$Sh = -\frac{1}{\delta}\left[\frac{\partial\phi(y,t)}{\partial y'}\right]_{y=0} \tag{32}$$

$$\left(1+\frac{1}{\beta c}\right)\frac{1}{L} = H, \frac{U_0^2}{\beta c^6 L} = \Omega$$

2.3 Similarity Transformations

Integrating equation (17) we have

$$v(y,t) = contant$$

At $y = 0$,

$$v(0,t) = s = contant$$

That is

$$v(y,t) = V_w \tag{33}$$

Define similarity transformations

$$\eta = \frac{y}{\sigma(t)}, u(t,y) = U_0 f(\eta), \theta(t,y) = g(\eta), \phi(t,y) = h(\eta) \tag{34}$$

Where

$$\delta(t) = \frac{\sigma_0}{\sigma(t)}$$

Equation (18) -(20) becomes

$$-\left(\eta\frac{\sigma(t)}{\nu}\frac{d\sigma(t)}{dt} - s\sigma(t)\right)f'(\eta) = \frac{\sigma(t)^2}{\nu U_0}\frac{dU}{dt} + \frac{\partial}{\partial\eta}\left(\left(\zeta - \gamma\theta(\eta)\right)f'(\eta)\right) + Grt(\theta(\eta) + N\phi(\eta)) - M\left(f(\eta) - \frac{U}{U_0}\right) \tag{35}$$

$$-\left(\eta\frac{\sigma(t)}{\nu}\frac{d\sigma(t)}{dt} - s\sigma(t)\right)\theta'(\eta) = \frac{1}{Pr}\left(\frac{\partial}{\partial\eta}\left(\left(\alpha + \varphi\theta(\eta)\right)\theta'(\eta)\right) + \pi Pr\left[Nb\left(\phi'(\eta)\theta'(\eta)\right) + Nt\left(\theta'(\eta)\right)^2\right] + \beta\theta(\eta)\right) \tag{36}$$

$$-\left(\eta\frac{\sigma(t)}{\nu}\frac{d\sigma(t)}{dt} - s\sigma(t)\right)\phi'(\eta) = \frac{1}{Sc}\phi''(\eta) + \frac{1}{Sc}\frac{Nt}{Nb}\theta''(\eta) + \Lambda\phi(\eta) \tag{37}$$

The left hand-side of equations (35)-(37) suggest that

$$\frac{\sigma(t)}{\nu}\frac{d\sigma(t)}{dt} \text{ is a constant} \tag{38}$$

Integrating (38), we have

$$\sigma(t) = \sqrt{2cvt} \tag{39}$$

Wlog, we take $c = 2$ in (39). This implies

$$\sigma(t) = 2\sqrt{vt} \tag{40}$$

And

$$s = \frac{v_w L}{U\delta(t)} \Longrightarrow s\sigma(t) = \frac{v_w L}{U\delta(t)}\sigma(t) = \pm v_0 \tag{41}$$

Substituting the expression for $U(t)$ and equations (40) and (41) into equations (35)-(37), we then have well-posed non-linear governing equations for Heat and Mass Transfer Effects on MagnetoHydroDynamic Flow of Nanoparticles with Buoyancy and Variable Viscosity and Thermal Conductivity given as

$$\frac{\partial}{\partial\eta}\Big(\big(\zeta-\gamma\theta(\eta)\big)f'(\eta)\Big)+(2\eta-v_0)f'(\eta)+Grt\big(\theta(\eta)+N\phi(\eta)\big) -M(f(\eta)-1)+G=0 \tag{42}$$

$$\frac{\partial}{\partial\eta}\Big(\big(\alpha+\varphi\theta(\eta)\big)\theta'(\eta)\Big)+Pr(2\eta-v_0)\theta'(\eta)+\beta\theta(\eta) \pi Pr\left[Nb\big(\phi'(\eta)\theta'(\eta)\big)+Nt\big(\theta'(\eta)\big)^2\right]=0 \tag{43}$$

$$\phi''(\eta)+\frac{Nt}{Nb}\theta''(\eta)+Sc(2\eta-v_0)\phi'(\eta)+\Lambda Sc\phi(\eta)=0 \tag{44}$$

And the corresponding boundary conditions (16) becomes

$$t<0:\quad f(\eta)=0,\theta(\eta)=1,\phi(\eta)=1 \qquad \text{for all } \eta$$

$$t\geq 0:\quad \begin{cases} f(\eta)=1,\theta(\eta)=1,Nb\dfrac{\partial\phi(\eta)}{\partial\eta}+Nt\dfrac{\partial\theta(\eta)}{\partial\eta}=0, & \text{at } \eta=0 \\ f(\eta)\to 0,\theta(\eta)\to 0,\phi(\eta)\to 0, & \text{as } \eta\to\infty \end{cases} \tag{21}$$

Heat and Mass Transfer at the wall under the similarity transformation (34) becomes

$$Skin-Friction: c_f=\big(\zeta-\gamma\theta(\eta)\big)\Big[Hf'(\eta)+\Omega\big(f'(\eta)\big)^3\Big]_{\eta=0}, \tag{45}$$

$$Nusselt\ Number: Nu=-\big[\big(\alpha+\varphi\theta(\eta)\big)\theta'(\eta)\big]_{\eta=0}, \tag{46}$$

$$Sherwood\ Number: Sh=-[\phi'(\eta)]_{\eta=0} \tag{47}$$

3. Method of Solution

The nonlinear system of coupled equations. The equations (42) – (44) are solved numerically using an efficient built-in method of MAPLE 2021, according to boundary conditions (21a&b). This command automatically converts the system of nonlinear equations into a set of initial value problems by employing the shooting technique and then solves the resulting system by using Runge-KuttaFehlberg method.

On a real-valued two-point boundary value problem (BVP), the dsolve command with the numeric option finds a numerical solution for the ODE or ODE system BVP. Dsolve automatically detects this type of BVP problem and applies the appropriate algorithm. To specify the BVP solver to be used, the optional equation method=bvp [traprich] was used. Richardson extrapolation enhancement is used in this procedure. Richardson extrapolation is often faster for enhancement techniques, while postponed corrections consume less memory on complex problems. As in our case, this solution method can handle BVPs with fixed, periodic, and even nonlinear boundary conditions. Our method generates an initial solution profile that satisfies the boundary conditions to a large extent. We next use the odeplot function to animate our solution curves acquired from a call to dsolve/output numeric's (dsn). A call to odeplot produces a PLOT data structure, which the plotting device renders.

4. Results and discussion

The flow of transient energy and concentration transport over a boundless moving vertical permeable flat sheet with chemical reaction, heat absorption/generation and suction has been formulated and solved analytically by asymptotic expansions. The following description is used to determine the impact of several established concepts on reactive fluid flow. Prandtl number values are defaulted to Pr = 0.71. (plasma). The default Schmidt number value is picked as (0.60) to denote the water vapour. All emerging terms are mainly selected as follows: $\zeta=1.2,\pi=0.8,\ \ Grt=5,\ \ M=4,\Lambda=0.5,\ \ \alpha=0.5,v_0=0.2,Nb=0.1,Nt=0.1,N=0.4,\beta=0.6$ and $\varphi=0.4$ except otherwise stated in each graph

Each term's impact on the mass, energy, and flow rate distributions is graphically depicted. It should be noted that $Grt>0$ and $Grt<0$ depict the cooling and heating surface, respectively. Also, $\Lambda<0$ and $\Lambda>0$ represent

generative and destructive chemical reactions, respectively. While $\beta < 0$ and $\beta > 0$ indicate heat generation and heat absorption, respectively.

4.1. Velocity distribution

Figure 2 shows how increasing the value of increases the velocity profiles. The velocity profiles of various Grashoff numbers are shown in Figure 3. The velocity profile grows as the value of Grashoff numbers rises. The velocity profiles in figure 4 grow as the value of N increases. Figure 5 shows that as the value of rises, the velocity profile rises as well. The influence of varying values of the magnetic field parameter M on the velocity profile is shown in Figure 6. The velocity profiles rise as the magnetic field parameter increases. The effect of the thermophoresis parameter on the velocity profile is seen in Figure 7. As the thermophoresis value increases, so does the velocity profile. Figure 8 shows how changing the Brownian motion parameter values increases the velocity profiles. Figures 9,10,11,12 and 13 with the parameters φ, ζ, α, v_0 G were displayed, and the graph shows that as the parameter increases, the velocity profiles increase as well.

4.2. Energy distribution

In figure 14, as the value of π increases it increase the temperature profiles. Figure 15 display the temperature profiles of different values of β. As the values of β increases, it increases the temperature profiles. The temperature profiles in figure 16 grow as the Brownian motion parameter value increases .Figure 17 shows that as the value of φ grows, so does the temperature profile. Figure 18 also shows temperature profiles for various values of v_0; when v_0 rises, the temperature profiles rise as well.

4.3. Concentration distribution

Figure 19 depicts the impact of various thermal conductivity values on concentration profiles. As the rises, the concentration profiles rise with it. Figure 20 depicts the effect of the v_0 parameter on concentration profiles. As the v_0 parameter increases, the concentration profiles increase as well. Variation of the Brownian motion parameter enhances the concentration profiles in figure 21.

Table 1: Effect of governing parameter on the flow

β	Grt	N	γ	π	Nb	Nt	φ	Λ	ζ	α	v_0	G	M	Sh	Nu	c_f
1.6														1.028608	-0.58537	0.18586
0.6												,		0.961347	0.223622	0.02596
-0.6														0.916149	0.733506	-0.00657
-1.6														0.887816	1.038846	-0.02336
	-5.0													0.961347	0.223622	-19.61017
	-2.0													0.961347	0.223622	-6.46006
	5.0													0.961347	0.223622	0.02596
	10.0													-0.04971	0.447391	0.33534
		0.2												0.961347	0.223622	-0.00735
		0.8												0.961347	0.223622	0.20647
		1.2												0.961347	0.223622	1.61000
		1.6												0.961347	0.223622	8.59219
			1.6											0.961347	0.223622	0.00597
			0.8											0.961347	0.223622	-0.00568
			0.2											0.961347	0.223622	0.00721
			0.0											0.961347	0.223622	1.39304
				0										0.942237	0.453775	0.00674

β	Grt	N	γ	π	Nb	Nt	φ	Λ	ζ	α	v_0	G	M	Sh	Nu	c_f
				0.8										0.961347	0.223622	0.02596
				1.4										0.9707	0.100508	0.04261
				2.0										0.980771	-0.06285	0.08761
					0									0.948096	0.410764	0.01813
					2.0									0.959051	0.076379	0.04633
					4.0									0.954565	-0.07617	0.09358
					6.0									0.951517	-0.11938	0.13764
						0.1								0.961347	0.223622	0.02596
						0.5								1.174607	0.119364	0.04741
						1.0								1.511341	0.029731	0.06840
						2.0								2.323813	-0.09867	0.08806
							0							0.967895	0.19897	0.01438
							0.2							0.958757	0.221508	0.03606
							0.4							0.956414	0.20651	0.05367
							0.8							0.954946	0.168805	0.09391
								-2.5						1.432228	0.21272	0.01589
								-0.5						0.961347	0.223622	0.02596
								0.5						0.641963	0.234846	0.03498
								2.5						-0.59641	0.31337	0.10006
									0.2					0.961347	0.223622	0.00000
									0.4					0.961347	0.223622	-0.00174
									0.8					0.961347	0.223622	-0.01725
									1.2					0.961347	0.223622	-0.03804
										0.1				0.980156	0.08796	0.01527
										0.5				0.961347	0.223622	0.02596
										1.5				0.951878	0.263732	0.04788
										2.5				0.949853	0.268809	0.05907
											-0.4			1.462999	0.775493	-0.20395
											-0.2			1.237	0.523203	-0.04136
											0.2			0.961347	0.223622	0.02596
											0.4			0.515927	-0.17822	0.20355
												-1.0		0.961347	0.223622	1.29884
												-2.0		0.961347	0.223622	0.52848
												-3.0		0.961347	0.223622	0.15856
												-4.0		0.961347	0.223622	0.02596
													4.0	0.961347	0.223622	0.02596
													4.5	0.961347	0.223622	0.03425
													5.0	0.961347	0.223622	0.04155
													5.5	0.961347	0.223622	0.04786

5. Conclusion

MHD Active Control Flow of Nanoparticles with Buoyancy and Variable Viscosity and Thermal Conductivity controlling equations were derived. The partial differential equations of the flow are reduced to a system of nonlinear ordinary differential equations, which are then solved using MAPLE 2021's shooting technique, and the Runge-kutta Fehlberg method is used to solve the resulting system. The current study reveals the following physical features of importance in terms of flow velocity, temperature, and concentration:

1. For air, increasing the Grashoff numbers results in a considerable increase in velocity distribution, whereas chilling the plate results in the opposite effect.
2. For destructive chemical reactions, the Lambda conductivity parameter rises while the concentration falls. Generous chemical reactions, on the other hand, have the opposite effect on the lambda conductivity number and concentration profiles.
3. Increase in velocity in the β parameter, which is a function of heat absorption and has the opposite effect on heat creation.

References

[1]. Yousefi, K. & Saleh, R. (2015). "Three-dimensional suction flow control and suction jet length optimization of NACA 0012 wing" (PDF). *Meccanica.* 50 (6): 1481–1494.

[2]. HadarBen-G. & Roi G. (2021): Application of passive flow control techniques to attenuate the unsteady near wake of airborne turrets in subsonic flow. *Aerospace Science and Technology. Volume* 119.

[3]. Omid E. & Khoshnam S. (2021): A novel model-free robust saturated reinforcement learning-based controller for quadrotors guaranteeing prescribed transient and steady state performance. *Aerospace Science and Technology, Volume* 119.

[4]. Syed T. M., Umar K., Naveed A. & Muhammad M. R.(2018) A study of heat and mass transfer on Magnetohydrodynamic (MHD) flow of nanoparticles Propulsion . *Power Research* 7(1):72–77

[5]. Hafiz A. W., Hussan Z., Saira B., Muhammad G., Seifedine K. & Yunyoung N. (2020). Numerical Study for the Effects of Temperature Dependent Viscosity Flow of Non-Newtonian Fluid with Double Stratification. *Appl. Sci. 10,* 708.

[6]. S.T. Mohyud-Din, U. Khan, N. Ahmed, Bandar Bin-Mohsin. (2017) Heat and mass transfer analysis for MHD flow of nanofluid in convergent/divergent channels with stretchable walls using Buongiorno's model, Neural Comput. *Appl*. 28 (12) 4079–4092.

[7]. U. Khan, N. Ahmed, S.T. Mohyud-Din, Stoke's first problem for carbon nanotubes suspended nanofluid flow under the effect of slip boundary condition, *Journal. Nanofluids* 5 239–244.

[8]. H. Schlichting, (1968) Boundary-Layer Theory, 6th ed., McGraw-Hill, New York.

[9]. K.R. Rajagopal, T.Y. Na (1983) On Stokes' problem for a non-Newtonian fluid,. 48, 233–239.

[10]. M. Turkyilmazoglu, (2015) Analytical solutions of single and multiphase models for the condensation of nanofluid film flow and heat transfer, *Eur. J. Mech. - B/Fluids* 53, 272–277.

[11]. M. Turkyilmazoglu (2012) Soret and heat source effects on the unsteady radiative MHD free convection flow from an impulsively started infinite vertical plate, *Int. J. Heat. Mass Transf*. 55 (25-26) 7635–7644.

[12]. G.S. Seth, M.S. Ansari, R. Nandkeolyar (2011) MHD natural convection flow with radiative heat transfer past an impulsively moving plate with ramped wall temperature, Heat. *Mass Transf.* 47, 551–561.

[13]. G.S. Seth, G.K. Mahato, S. Sarkar, M.S. Ansari (2012) Effects of Hall current on hydromagnetic natural convection flow of a heat absorbing fluid past an impulsively moving vertical plate with ramped temperature, *J. Appl. Fluid Mech*. 1 (4) 462–486.

[14]. G.S. Seth, R. Nandkeolyar, M.S. Ansari (2013) Effects of thermal radiation and rotation on unsteady hydromagnetic free convection flow past an impulsively moving vertical plate with ramped temperature in a porous medium, *J. Appl. Fluid Mech. 6* (1) 27–38.
[15]. R. Nandkeolyar, G.S. Seth, O.D. Makinde, P. Sibanda, M.S. Ansari, (2013) Unsteady hydromagnetic natural convection flow of a dusty fluid past an impulsively moving vertical plate with ramped temperature in the presence of thermal radiation *ASME J. Appl. Mech.* 80 (6)
[16]. G.S. Seth, S. Sarkar, S.M. Hussain, Effects of Hall current, radiation and rotation on natural convection heat and mass transfer flow past a moving vertical plate, Ain Shams Eng. J. 5 (2014) 489–503.
[17]. G.S. Seth, S. Sarkar, S.M. Hussain, G.K. Mahato (2015) Effects of Hall current and rotation on hydromagnetic natural convection flow with heat and mass transfer of a heat absorbing fluid past an impulsively moving vertical plate with ramped temperature, *J. Appl. Fluid Mech.* 8 (1) 159–171.
[18]. G.S. Seth, S. Sarkar(2015) MHD natural convection heat and mass transfer flow past a time dependent moving vertical plate with ramped temperature in a rotating medium with Hall effects, radiation and chemical reaction, *J. Mech*. 31 91–104.
[19]. G.S. Seth, S. Sarkar, R. Sharma (2016) Effects of Hall current on unsteady hydromagnetic free convection flow past an impulsively moving vertical plate with Newtonian heating, *Int. J. Appl. Mech. Eng*. 21 (1) 187–203.
[20]. G.S. Seth, S. Sarkar (2015) Hydromagnetic natural convection flow with induced magnetic field and nth order chemical reaction of a heat absorbing fluid past an impulsively moving vertical plate with ramped temperature, Bulg. 47 (1) 66–79.
[21]. V.M. Soundalgekar (1981) Stokes problem for elastico-viscous fluid, Rheol. Acta 13, 177–179.
[22]. P. Puri (1984) Impulsive motion of a flat plate in a Rivlin-Ericksen fluid, Rheol. Acta 23, 451–453.
[23]. P. Puri, M. Jordan (1999) Stokes's first problem for a dipolar fluid with non-classical heat conduction, J. Eng. Math. 36, 219–240.
[24]. H. Rosali, A. Ishak, I. Pop (2014) Stokes' first problem in nanofluids, Curr. Nanosci. 10 409–413.
[25]. N. Uddin, W.A. Khan, M. Rahi (2012) Heat and mass transfer from a suddenly moved plate in nanofluids, Proc. Inst. Mech. Eng., Part N: J. Nanoeng. Nanosyst. 1–9.
[26]. D.A. Nield, A.V. Kuznetsov (2014) The onset of convection in a horizontal nanofluid layer of finite depth: a revised model, Int. *J. Heat. Mass Transf.* 77, 915–918.
[27]. D.A. Nield, A.V. Kuznetsov, (2014) Natural convective boundarylayer flow of a nanofluid past a vertical plate: a revised model, *Int. J. Therm. Sci.* 77, 126–129.
[28]. D.A. Nield, A.V. Kuznetsov (2014) Thermal instability in a porous medium layer saturated by a nanofluid: a revised model, *Int. J. Heat. Mass Transf.* 68, 211–214.
[29]. Habibnia M. and Pascoa J. (2021) Active Control Assessments towards Optimizing the Performance of a Cycloidal rotor at Hover. Aerospace and Technology.